Ghiasi and Lee
Advances in Bridge Engineering (2024) 5:14
https://doi.org/10.1186/s43251-024-00125-5

Advances in
Bridge Engineering

ORIGINAL INNOVATION Open Access

Estimation of nosing load in existing railway transom top bridges based on field testing and finite element modelling

Alireza Ghiasi[1,2*] and Daniel Lee[1]

*Correspondence:
aghiasi@ARTC.com.au

[1] The Australian Rail Track Corporation (ARTC), Adelaide, SA, Australia
[2] The University of Adelaide (UoA), Adelaide, SA, Australia

Abstract

A significant number of wind bracings in existing railway transom top bridges are numerically assessed deficient against the assessment nosing load recommended by the AS5100, where in almost all cases, there is no observed evidence of wind bracings being overloaded. This paper estimates the nosing load applied by various trains to a couple of random spans of an existing railway transom top bridge. Firstly, field testing of this bridge is conducted and the measured stresses at the mid-center of girders and wind bracings are collected during various normal train operations to validate the developed Finite Element (FE) models of this bridge. Then, the nosing loads due to different trains are estimated using the validated FE model through a two-staged validation approach, including automatic FE stress intensity optimization and rigorous manual FE model sensitivity analysis while transoms in various conditions are also incorporated in the FE model. Results demonstrate that the nosing load is significantly less than the required load in the AS5100 with magnitudes ranging between 8.6% to 9.4% of the maximum vertical axle load of the passed trains; suggesting that the AS5100 assessment nosing load should be revised to avoid unnecessary expensive upgrades of numerically assessed deficient wind bracings.

Keywords: Railway transom top bridges, Nosing load estimation, FE model, FE model validation, AS5100

1 Introduction

Many timber transom top bridges in railway networks exist worldwide (Mirza et al. 2019). Thus far, these railway bridges have shown to be resilient against various train service loadings. In bridge design or assessment, most codes require that bridges be designed and assessed with an identical high lateral nosing load. This causes the majority of the existing wind bracings in the transom top bridges to be numerically assessed deficient mainly due to the lack of bracings' bending capacity against excessive induced compression force of the applied design nosing load. As a result, many bridge authorities consider extensive and expensive wind bracing upgrades or strengthening to make these bridges compliant with the current bridge design codes whilst there is no sign of distress in almost all of these wind bracings.

In railway bridge design, there are three major designs; transom top, ballast top, and directly fixed track bridges (AS5100.2, Bridge Design Part 2: Design loads 2017). Most railway transom top bridges are simple bridges comprising two girders connected using low-capacity wind and sway bracings, in which timber (hardwood) transoms sit on top of the girders to carry rails and form an open deck railway bridge structure. The running rails are fixed directly to the transoms with an offset to the top of the girder flanges (AS7636, Railway Structures 2022). This offset makes imperfections in the track to the girder and the railway vehicles, therefore, the wheel flanges cause forces to transverse to the railway bridge axis. If such a lateral force and, accordingly, lateral displacement is excessive, the stability of the train can be affected and concerns can be raised about operation and safety (Moreu and LaFave 2012; Moreu et al. 2023). Although this lateral force is applied anywhere along the tracks i.e., even where there is no bridge in the rail network; the accurate calculation of applied stresses to the internal wind bracings in the railway transom top bridges is more important as these bridges are open deck type structures and there is no external stiff structural member such as deck slab to add capacity to the lateral resistance of the bridge and assist in reducing the stresses due to the nosing load. Indeed, the accurate determination of the actual added lateral capacity of transoms in an open deck bridge is difficult, because their condition, age, cross-section, and technical serviceability requirements can vary significantly from one place in a bridge to another as well as from one rail authority to another (ETE-09–00, Sect. 9: Structures 2023; TMC 2010; Part 1030 1030 2007). Figure 1 shows a transom top bridge with timber transoms in very different conditions from visually fair to very poor. It can be seen how the condition can vary from one place to another making such a capacity assessment very debatable by bridge engineers.

Ballast top bridges consist of decks that can add a level of medium to very high lateral stiffness to the bridge system depending on the deck's stiffness, connections, and composite or non-composite construction. Also, the ballasted track itself can add a very high level of additional lateral resistance depending on the degree of mechanical interlocking between the ballast particles and track condition (Khatibi et al. 2017; Resistance and of Railroad Track, U.S. 1977; Zakeri 2012; Prud'homme 1967). Hence, a bridge engineer may not be required to determine an actual nosing load applied to these bridges as these

Fig. 1 Example of timber transoms in a bridge in very different conditions from fair to very poor

bridge systems might readily take the design nosing force required by the bridge codes. A final structural assessment of an open deck or transom top bridge with no ballast, however, mostly recommends very extensive and expensive wind bracing replacement or upgrade due to reduced load rating factors (ETE-09–00, Sect. 9: Structures 2023). Reduction in load rating factors may also impose mass and speed restrictions on bridges and reduce the overall efficiency of the rail network while the magnitude of the actual nosing load is unknown by rail authorities. In the design and assessment of any railway bridge including the transom top structures, the nosing force needs to be taken as a concentrated force acting horizontally, at the top of the rails in either direction (Fig. 2 (AS7636, Railway Structures 2022)), perpendicular to the centreline of the track.

Originally, the general features of design and assessment, loadings, allowable stresses, etc., for all railway bridges including transom top bridges were controlled by the specifications of the American Railway Engineering and Maintenance-of-Way Association (AREMA) while the materials and specific additional documents of railway bridge constructions were provided by railway associations such as the International Union of Railways (UIC). For European standards, technical indications are given in Eurocode (Manual and Chapter 38, 2019; Pipinato and Patton 2015). The bridge design and assessment principles of the Australian Bridge Design Code, AS5100, consider 300LA traffic loading (i.e., four 300 kN axle loads including a simulated locomotive with a single axle load of 360 kN). This design standard is based on the Ultimate and Serviceability Limit States (ULS and SLS) aligning with the limit state design levels in Eurocode EN 1991–2: Eurocode 1 (AS5100.2, Bridge Design Part 2: Design loads 2017; EN 2006; AS5100.7, Bridge Design Part 7: Bridge Assessment 2017). For the maximum axle load of 445 kN, AREMA (Engineering et al. 1997) recommends a single point lateral load equivalent to 111.3 kN should be applied to the top of rails i.e., 25% of the maximum vertical axle load. Table 1 tabulates some important design codes and the mandatory requirements for nosing load applications to bridges.

As can be seen from Table 1, in practice, the bridge engineers would assess existing bridges for ULS nosing loads ranging from lower to very high loading requirements

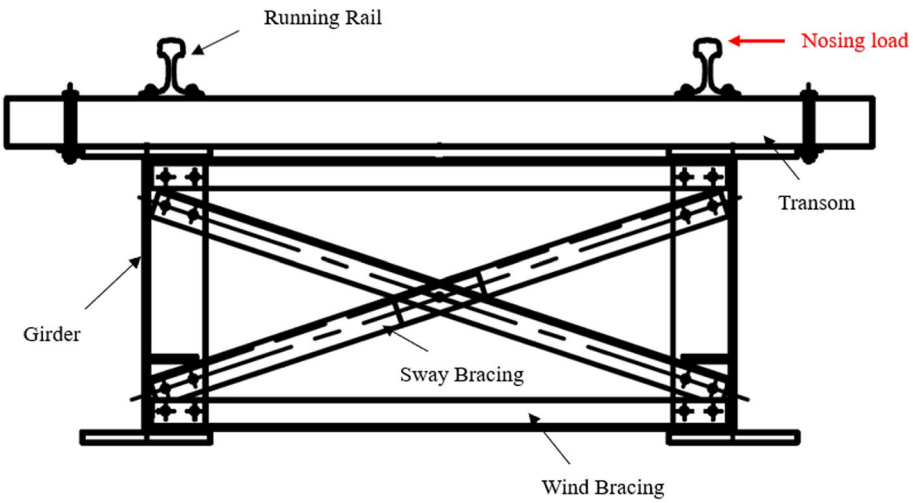

Fig. 2 Application of nosing load on railway transom top bridges

Table 1 Nosing load requirements in some bridge design codes

Design Code	Bridge Design	Bridge Assessment	Load Factor	Applied Nosing load for a 300 kN Vertical Axle Load	Specific Design Requirements
AREMA (Engineering et al. 1997)	25% of the heaviest axle load	25% of the heaviest axle load	Allowable Stress Design (ASD) (See Note 1)	300 × 0.25 = 75 kN	The effects of the lateral load should be disregarded in considering lateral bending between brace points of flanges, axial forces in flanges, and the vertical forces transmitted to the bearings
Eurocode (EN 2006)	100 kN	100 kN	ULS Load factor = 1.21 (Classified vertical loads)	100 × 1.21 = 121 kN	The nosing load shall not be increased by changing speed, or shall not be applied together with centrifugal force or with a Dynamic Load Allowance (DLA)
AS5100: 2017 (AS5100.2, Bridge Design Part 2: Design loads 2017; AS5100.7, Bridge Design Part 7: Bridge Assessment 2017)	100 kN	100 kN	ULS Load factor = 1.6	100 × 1.6 = 160 kN	

Note 1-In ASD, the maximum stress in a structural member should not exceed a certain allowable stress in the service conditions. The allowable stress of a material is determined according to its nominal material strength in elastic limit with a safety factor

as the prescribed values in different standards vary significantly. In Australia using AS5100.7 (AS5100.7, Bridge Design Part 7: Bridge Assessment 2017), where designers assess the existing transom top bridges using a point load of 160 kN for 300LA or e.g., 133.3 kN for 250 kN axle load ($25/30 \times 100$ kN $\times 1.6 = 133.3$ kN), a significant number of the existing wind bracings would numerically fail (axial compressive) under such a high required assessment load (this load is more than double higher than the design level that AREMA requires for the assessment of existing bridges), where almost in all cases, there is no evidence from the visual inspection that these wind bracings have been overloaded (ETE-09–00, Sect. 9: Structures 2023; Hr and CI 12008 ST 2019). It makes sense if the provision for a bridge design is adopted conservatively from the beginning for new bridge designs where there is no significant cost in providing stronger sections, however, for existing bridge assessments, there is a need to assess the existing bridges closer to reality to avoid unnecessary and costly maintenance in railway bridges.

Overall, previous research performed on the assessment of nosing load applied to bridges is very limited and needs to be more focused by engineers or researchers as it can significantly impact bridge maintenance costs in railway organizations. Georgiev et al. (Georgiev et al. 2021) investigated the nosing load applied by some trains to a steel transom top bridge in Bulgaria and compared the stresses obtained from the field testing with the stresses obtained from a simple grillage model. They did not validate their grillage model but only used that model as a baseline to estimate the design stresses. Their field testing results revealed that the design requirements as per Eurocode were too conservative being three to four times higher than the actual field testing loads for the tested transom top bridge. Their obtained nosing load values were a maximum of 14 kN for passenger trains and 30 kN for heavy freight trains, however, they did not mention

the vertical axle loads for tested freight and passenger trains. Moreu et al. (Moreu et al. 2023) investigated nosing loads and displacements for some existing railway bridges using three different gauging systems including a Truck performance Detector (TPD), a Track loading Vehicle (TLV), and Linear Variable Differential Transformers (LVDT). As per the field measurements, they concluded that field monitoring is a better approach than using conservative values in any design code for determining the nosing load. In their study, they showed that the simplification of a single concentrated lateral force as per Eurocode was a very conservative assumption that did not represent the realistic lateral load distribution on existing bridges. The authors also concluded that the majority of the recorded lateral forces from freight operations were much lower than the recommended design values in AREMA. Otter et al. (Otter et al. 2005) investigated the net truck lateral forces using load-measuring wheelsets and wayside measurements from TPD and Wheel Impact Load Detector (WILD) to review the lateral force guidelines used in AREMA for the rating of steel bridges. In their report, they mentioned that the maintenance of lateral bracing members in open-deck steel railway bridges is a major portion of the overall railway bridge maintenance budget. Their actual field data revealed that 95% of the recorded lateral forces in all open-deck bridges were less than 26.7 kN. Their wayside data also showed that 99.95% of the recorded lateral forces were less than 66.7 kN at most of the locations due to vertical axle loads of up to 293.6 kN e.g., the ratio of the highest measured net truck lateral force to nominal vertical axle load was about 20% to 25%, in agreement with the AREMA recommendation for steel bridge design. The authors' proposed future plans should include measurements of strains or stress in various wind bracing members of steel bridges to help quantify the actual axial and bending forces in bracing members. UIC-D181 Committee (James and Scott 1994) reported that the peak lateral displacements of tracks were greatly affected by track irregularities and wheel conicity meaning that the poorer the tracks and wheels are maintained, the greater the peak lateral force on the track was. The research committee obtained peak lateral displacement of rails using structural simulations of a 120-m long span of a bridge were around 0.02 m which corresponded to 54 km/hr of train speed. This simulation, however, was not tested in practice. In separate research on UIC-D181 Committee findings, Deng (Deng 2015) concluded that the peak lateral displacements obtained by UIC-D181 Committee's simulations were too conservative meaning that the UIC-D181 overestimated the nosing load and the obtained 0.02 m lateral displacement was very high.

Other than the actual expensive field tests conducted by Otter et al. (Otter et al. 2005) which covered hundreds of kilometers of track in America loaded by nearly ten million trucks to record the nosing loads, none of the other research measured the nosing loads applied to transom top bridges due to various trains at different speeds. Lack of actual field test data results in overestimating the nosing load in desktop assessment problems and increases the cost of required maintenance works. Conducting e.g., expensive TPD and WILD require rail-mounted sensors at various locations, however, these sensors may not be available or financially justified in all the locations along the tracks. This paper introduces a novel way of nosing load estimation using FE model updating and temporary field testing where no permanent sensing equipment is available at a bridge.

The results from this paper can assist bridge engineers in desktop assessment as well as suggest to AS5100 to revise the nosing load assessment requirements.

The approach taken to estimate the nosing load is represented in Fig. 3. This paper is organized as follows: Firstly in Sect. 2, the field testing of the in-service railway bridge, the Menindee Darling River Railway Bridge, is elaborated. In Sect. 3, developed FE models of the bridge are described in detail from the development to the initial results acquisition. In Sect. 4, nosing load estimation is explained in detail which includes a two-staged model validation approach including both the automatic stress intensity optimization and manual FE model sensitivity analysis. Finally, in Sect. 5, the nosing loads are estimated for each tested train, results are discussed for various transom conditions, and recommendations for AS5100.7 (AS5100.7, Bridge Design Part 7: Bridge Assessment 2017) and improvements are presented.

2 Field testing

2.1 Description of the Menindee darling river railway bridge

The Menindee Darling River Railway Bridge (Fig. 4) is located in Menindee, far west of New South Wales in Australia, over the Darling River on the Australian Rail Track Corporation (ARTC)'s railway track. This bridge was constructed Circa 1926. The total length of this long bridge is 235.2 m comprising 28 nominal 8.4-m long spans. All the spans are simply supported comprising typical timber transom top (open deck) steel girders connected together using wind and sway bracings. It is known that this bridge is a typical open deck structure representing thousands of similar spans that are currently in service on all railway tracks worldwide. The bridge is in good condition only with some minor signs of rusting on the steel members with no visible distressed members anywhere as inspected during the field testing week. Transoms are visually inspected for these spans and found to be in reasonable condition.

2.2 Instrumentation

In August 2023, two random spans are selected for field testing (span numbers 1 and 5). Six BDI strain transducers (gauges) for each span (12 in total, see Fig. 5) are installed at the measured center of members to collect the stresses due to normal train operations in a week. The girders of this bridge are rated with adequate capacity for a 250 kN axle load of ARTC's nominated rating trains (ETE-09–05, Sect. 9: Load Rating of Underbridges 2022) and there are no speed or mass restrictions when the testing is conducted. The diagonal wind bracings are $3 \times 3 \times 3/8''$ ($76.2 \times 76.2 \times 9.525$ mm) equal angles with 2.84-m long at which A/B3, A/B5, and A/B6 strain gauges are installed.

During the field testing week, the strain data for eight random freight trains with various axle loading and spacing between axles is collected for each strain gauge. It is noted that more trains are reported passing over this bridge during the field testing week, however, only trains that accurate data could be extracted from ARTC wayside monitoring are discussed in this paper. Figure 6 shows the information on axle loading (kN) for each train. Table 2 tabulates the number of recorded axles for each freight train including locomotives (with 6 axles) and wagons/containers (with 4 axles). Figure 7 shows a sample photograph of Train 3SP7 passing over the bridge.

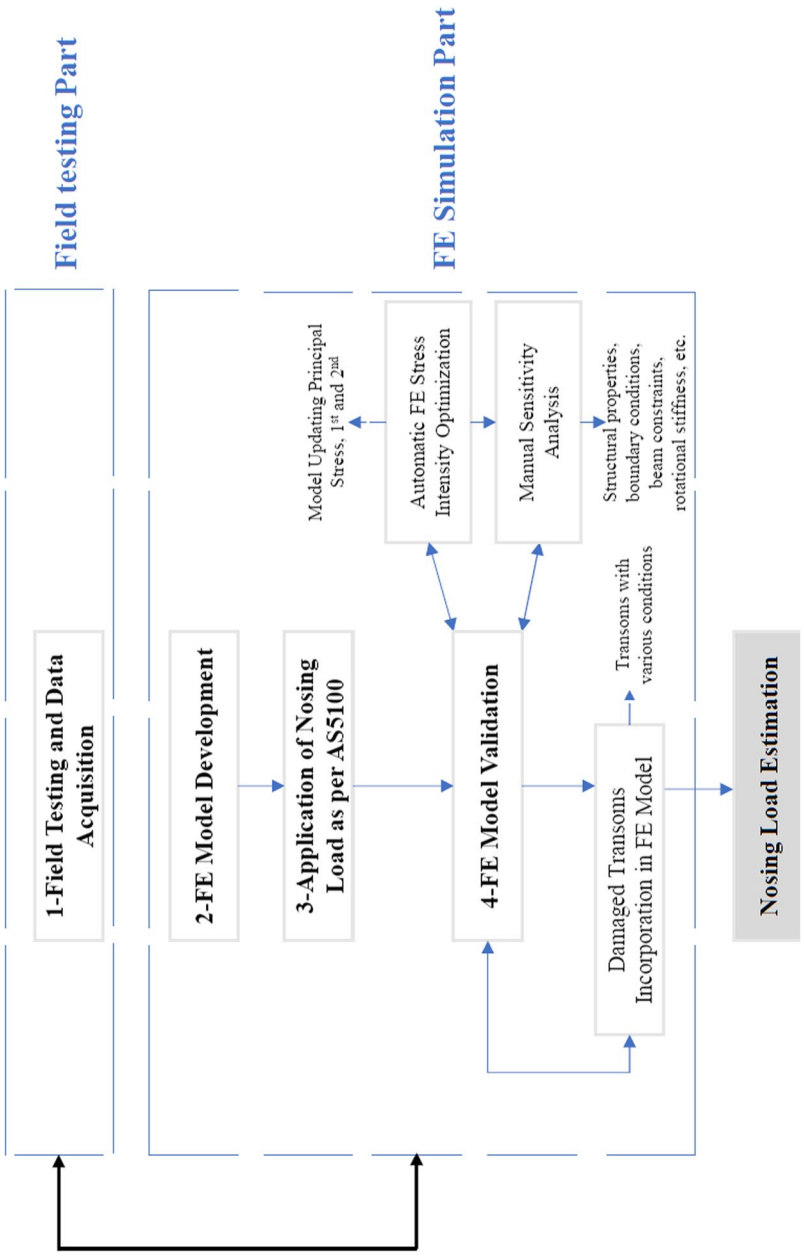

Fig. 3 General flowchart of nosing load estimation

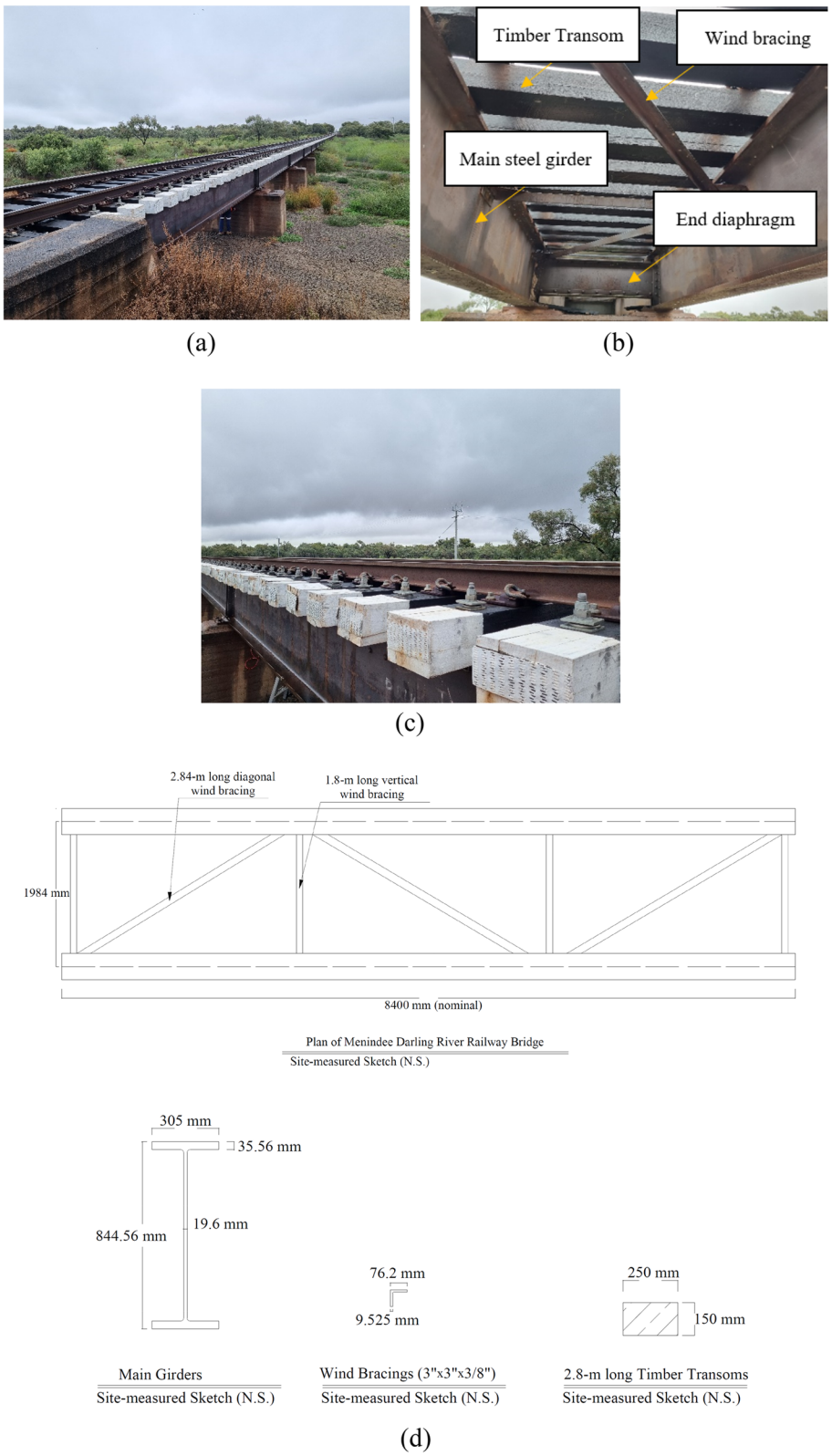

Fig. 4 (**a**) General view of the Menindee Darling River Railway Bridge, (**b**) Underside of spans, (**c**) General view of timber transoms, and (**d**) Site-measured sketches of the bridge and members' cross-sections

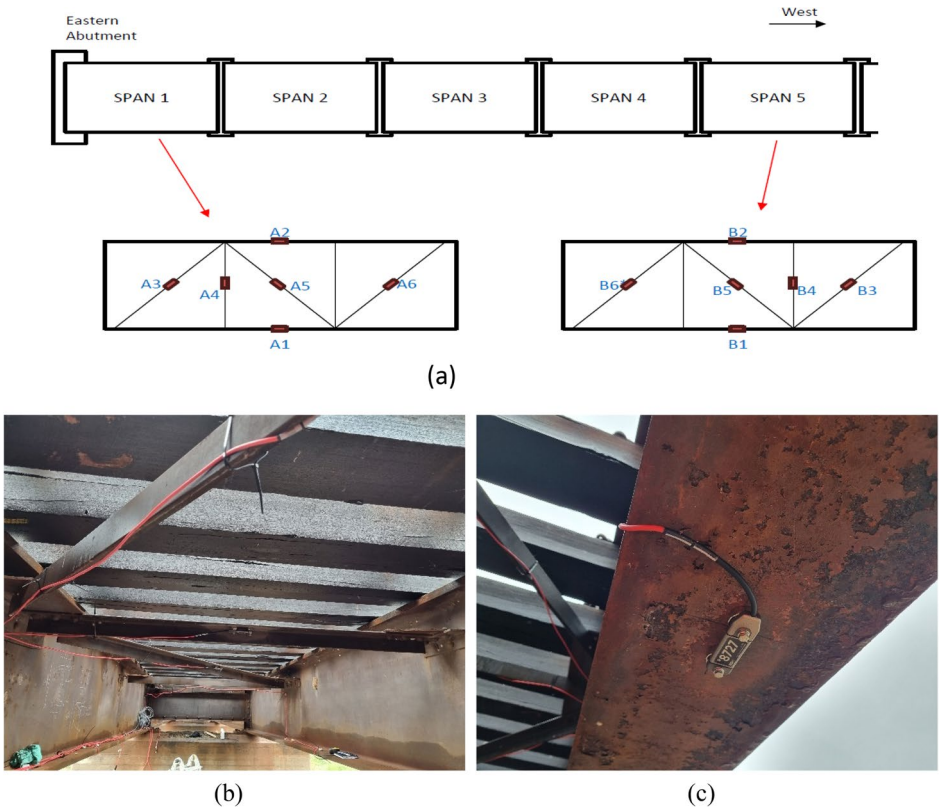

Fig. 5 (**a**) Schematic of strain gauge locations, (**b**) strain gauging of spans, and (**c**) view of a strain gauge

The strain data are recorded in units of microstrain (με). For better presentation of data, the simple Eq. (1) is used to obtain the tensile or compressive stresses in the linear elastic region using Young's Modulus of steel material as below (Jastrzebski 1959):

$$\sigma_f = E.\varepsilon_f \tag{1}$$

where σ_f is the scalar matrix of the field-recorded tensile or compressive stress (MPa) in the f direction of an element plan,E is the Young's Modulus (MPa), and ε_f is the scalar matrix of the field-recorded strain ($\mathrm{m/m} = \mu\varepsilon \times 10^6$) in the same direction. All the matrices E for steel material is taken as 200,000 MPa. Figure 8 shows an example of the recorded stresses for train 4YN2 in different members (refer to strain gauges index, Fig. 5). The field-recorded stress data due to other trains' passage is not published in the paper to reduce the number of shown Figures. All recorded stress data shows that the highest-speed train, 3NY3, does not induce the highest stresses to the girders due to the reason that the load intensity of this train is not the highest. The positive and negative stresses represent compressive and tensile stresses, respectively, in all the Figures.

The maximum recorded tensile stresses at the bottom of girders (at mid-span) is 44.2 MPa (train 3YN2) with the highest load intensity and it relates to Span 5. In all trains, the bottom of girders at mid-span of Span 5 show relatively higher tensile stresses than Span 1 (between 3 to 8% higher) which can be due to the marginally longer span (8.4-m long span is nominal but many inspections reveal that some old spans can be marginally longer or shorter). South girders and north girders also show marginally different

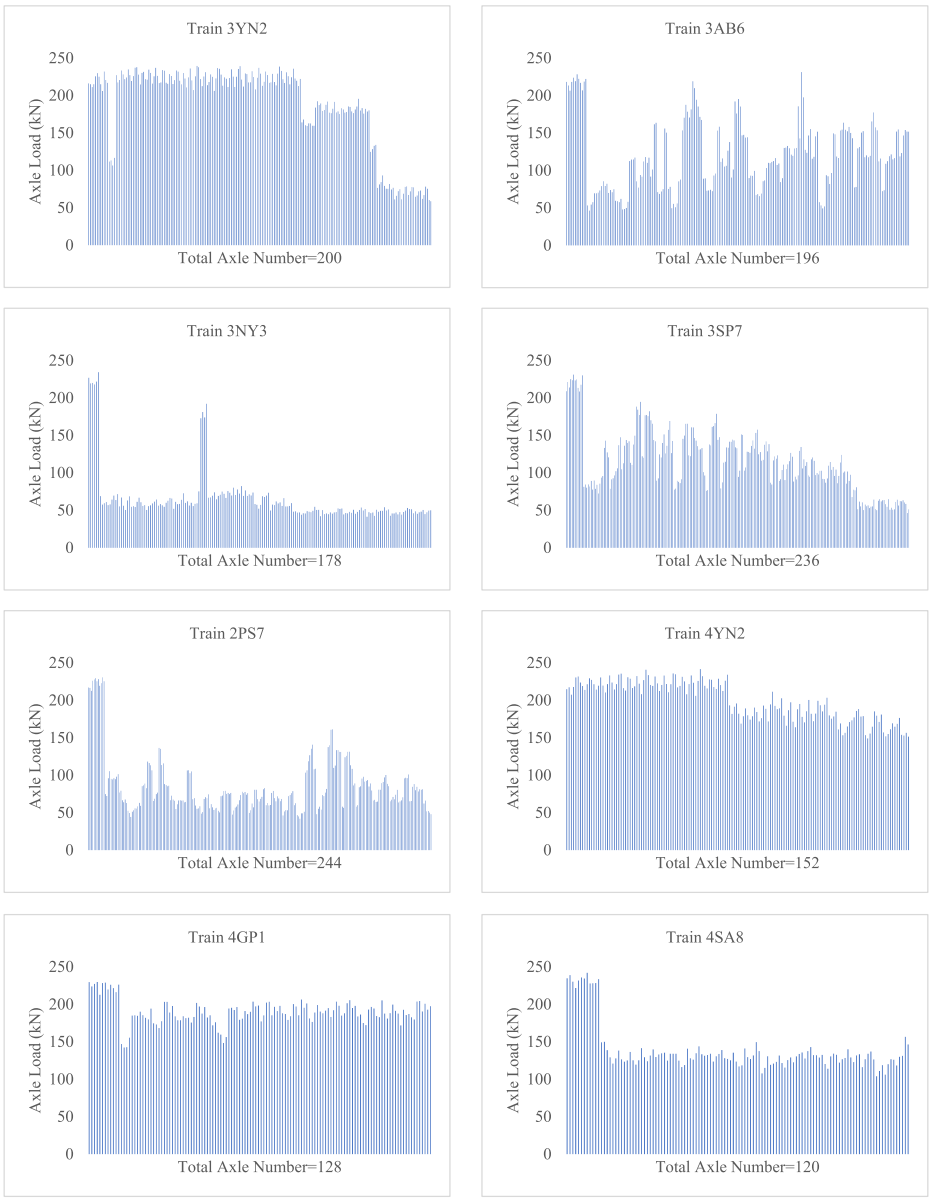

Fig. 6 Trains and their actual axle loads

Table 2 Number of axles for each passed train (including locomotives and wagons/containers)

Train index	Total Number of Axles	Total Number of Locomotive Axles	Total Number of Wagon/Container Axles	Recorded Train Speed at the bridge (km/h)
3YN2	200	2 × 6 = 12	47 × 4 = 188	28
3AB6	196	2 × 6 = 12	46 × 4 = 184	27
3NY3	178	1 × 6 = 6	43 × 4 = 172	61
3SP7	236	2 × 6 = 12	56 × 4 = 224	37
2PS7	244	2 × 6 = 12	58 × 4 = 232	28
4YN2	152	2 × 6 = 12	35 × 4 = 140	30
4GP1	128	2 × 6 = 12	29 × 4 = 116	52
4SA8	120	2 × 6 = 12	27 × 4 = 108	32

Fig. 7 Train 3SP7 passing over the bridge

stresses as expected as most of the freight trains can marginally be loaded unequally. The recorded compressive and tensile stresses in all the bracing members are very low (compressive all < 10.2 MPa and tensile all < 12.6 MPa with the majority < 8 MPa). The maximum recorded axle load among the eight trains is 242 kN belonging to trains 4SA8 and 3YN2 (Fig. 6) which necessitates a design of a point nosing load to $242/300 \times 100$ kN = 80.7 kN according to AS5100.2 (AS5100.2, Bridge Design Part 2: Design loads 2017). In Sect. 3, the FE simulations are developed, checked, and validated for this bridge.

3 Finite element simulation

3.1 Model development

Two three-dimensional FE models of the Menindee Darling River Railway Bridge are developed using the commercially available software Space Gass. FE Model 1 (Fig. 9(a)) is carefully developed using triangular or quadrilateral plate/shell elements with six Degree-of-Freedom (DoF) for all the steel members of the bridge including girders, end diaphragms, all bracings, and their connections without modelling of the track while FE Model 2 (Fig. 9(b)) also includes timber transoms and 53 kg rail profiles (AS 1085.1 2002) modeled as beam elements with accurate offsets as measured at the site. Both models are simply supported at the bottom flanges at the end supports. In FE Model 2, the span includes 19 timber transoms measured to be varied between 0.45 to 0.5 m center-to-center distance from each other. As the stress validation is the target within the material elastic zone and the bridge is rated adequately for the 250 kN axle loading, the material behavior and geometric for steel finite plate elements, timber, and rail members are all set as linear without any loading imperfections. This is aligned with AS5100.6 (AS5100.6, Bridge Design Part 6: Steel and Composite Construction 2017) recommendations on rigorous structural analysis of elastic resistance of existing bridges. For FE Model 2, the timber transom members are initially modeled with the model's default beam constraints/fixities with DoF of FFFFFF (fixed) for translations and rotations in all directions. Beam constraints/fixities specify how beam elements are connected to FE plate/shell nodes. This is different from how beams are connected to supports (boundary conditions). Beam constraint should carefully be altered in a model until it can simulate

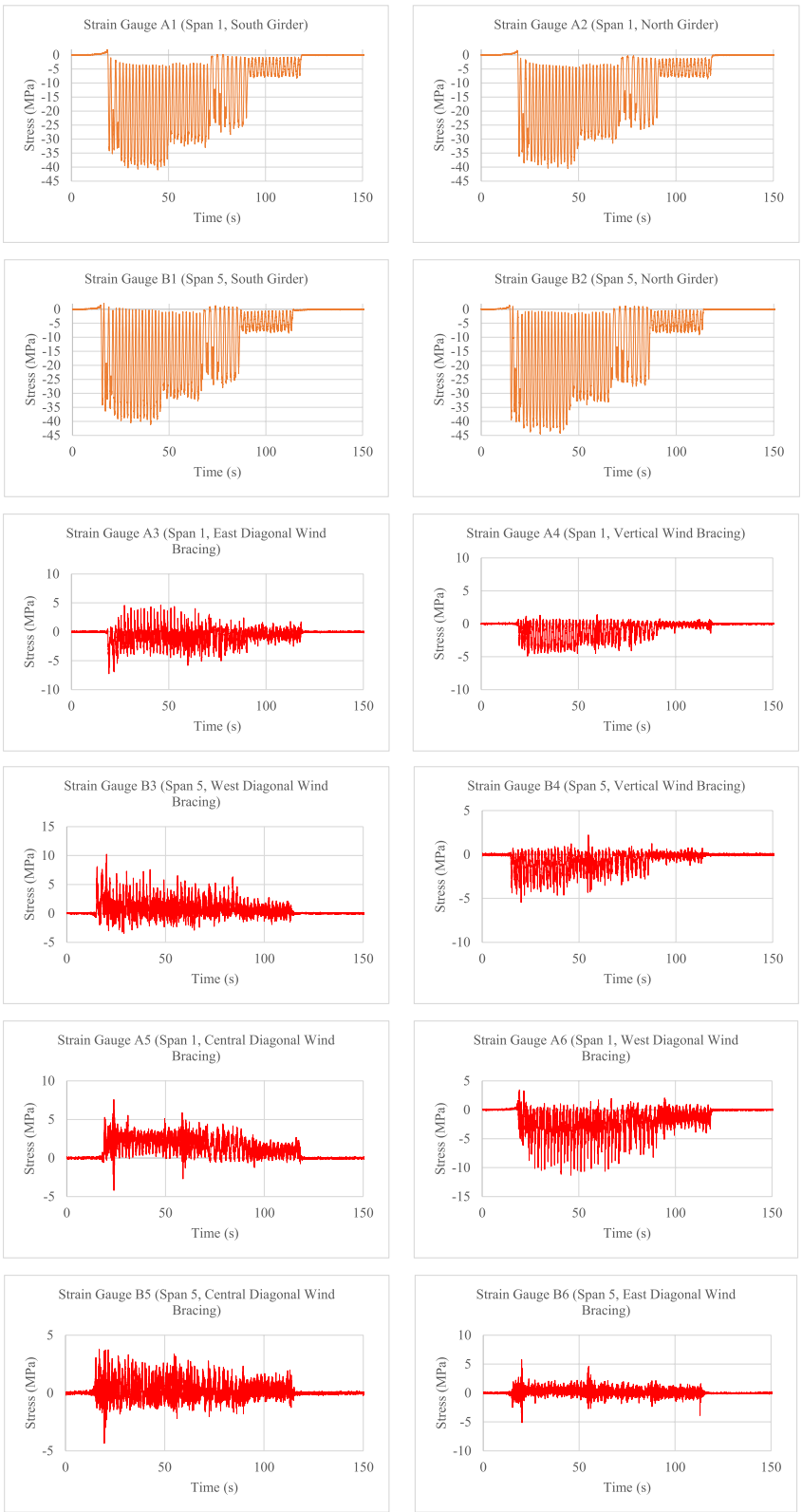

Fig. 8 Field-recorded stresses at elements (center of the members) of Spans 1 and 5 due to the passage of train 4YN2-Refer Fig. 5 (**a**) for strain gauges index

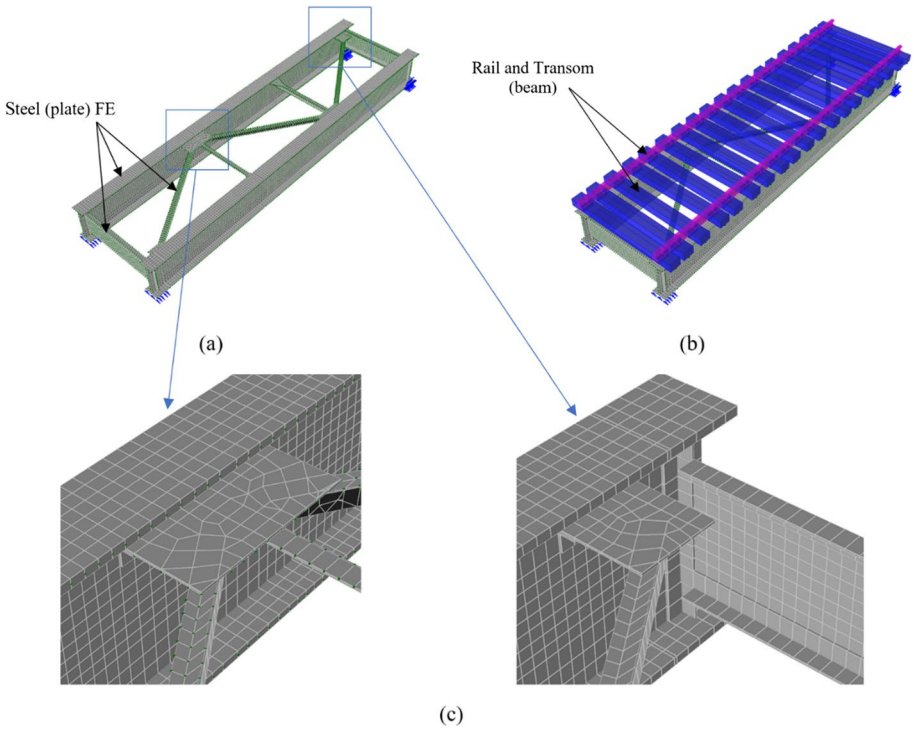

Fig. 9 FE models of Menindee Darling River Railway Bridge (**a**) Model 1-model without rails and timber transoms (only the steel bridge) i.e., loads are directly applied on top of FE girders' flanges elements, (**b**) Model 2-model including rails and timber transoms i.e., loads are applied to the rail members, and (**c**) detail of girder, bracings, end diagrams and connections (All elements are shown as rendered for clarity)

true behaiviour of connections. This is further investigated in Sect. 4. The beam elements have six DoF per node, so they are connected with other plate FE elements node-to-node with no further modelling requirements. Miri (Miri 2022) investigated the best fastening strategy for transom modelling in an FE model to represent existing open deck transom top bridges and resulted in them being modeled as fully bolted to match the common practice in the industry (Case FP1 in their study i.e., resilient fasteners with the nominal transom spacings of 0.5 m), however, it is believed that in their study, they only considered longitudinal effects in railway bridges which did not align with the current modelling approach or the current problem to be solved. Indeed as mentioned in Sect. 1, adopting true constraints for each transom is difficult in practice without more detailed field testing; as timber transoms may widely vary in boundary conditions, true member stiffnesses, and conditions from one transom to another. The purpose of developing both FE Models is to obtain the maximum numerical 1st and 2nd principal stresses (Mohr's Circle, 1882) due to the combination of design vertical and lateral load to the bridge.

It is worth mentioning that all eight trains (including locomotives and wagons/containers) in Fig. 6 are accurately modeled with the same axle/wheel loadings and the same axle spacing provided by the ARTC wayside monitoring. For modelling nosing loads, initially, a single moving lateral point load adjusted by the ratio of the maximum axle load in each train is applied as per AS5100.2 (AS5100.2, Bridge Design Part 2: Design loads 2017) (e.g., for a train with a maximum 242 kN axle load, a single moving point lateral load equal to $242/300 \times 100$ kN $= 80.7$ kN is applied). It is advised by the wayside

monitoring that the axle loading may have an error of up to ± 3%, while the spacings are accurate as per rolling stock datasheets. Table 3 lists the material properties of steel and timber transoms as modeled. Figure 9 shows some snapshots of the FE Models 1 and 2.

3.2 Model validation and results

Both FE Models 1 and 2 are analyzed in linear static moving load analysis for all the tested trains in SLS (with a load factor of unity) and ULS (with a load factor of 1.6 as per AS5100.2 (AS5100.2, Bridge Design Part 2: Design loads 2017)) both with and without recommended applied Dynamic Load Allowance (DLA) as per AS5100.2 (AS5100.2, Bridge Design Part 2: Design loads 2017) to validate the models stresses and DLA for the spans. DLA is a common denomination of dynamic indices (McLean 1998) that would be applied to the static loads to simulate dynamic effects on bridges' structural members which depend on the characteristic length of the structural member of bridges and vehicle speed at any time. It should be noted that in the coupled vehicle-bridge vibration analysis, the wheel-rail interaction forces are time-varying and cannot be simplified to a constant value. However; in the absence of a more detailed analysis for each vehicle; AS5100.2 (AS5100.2, Bridge Design Part 2: Design loads 2017) recommends increasing static effects by applying DLAs to various static loads to obtain approximate dynamic effects in each case. No DLA should be applied to nosing loads as advised by all design codes (i.e., nosing load should be used as a static effect). In SLS analysis, DLAs in each model change following the speed recorded in Table 2 as per AS5100.7 (AS5100.7, Bridge Design Part 7: Bridge Assessment 2017). For example, the maximum standard DLA (bending) for a nominal 8.4-m long span is 0.52 for a speed of ≥ 80 km/h as per AS5100.2 (AS5100.2, Bridge Design Part 2: Design loads 2017). In the SLS check, this DLA would only be taken as 0.4 for the maximum speed of 61 km/h for stress validation in the FE models ($0.2 < DLA < 0.67$). In ULS, this DLA is taken for full speed i.e., the value of 0.52. Figure 10 shows some sample contour stress mapping of the analyzed FE Models 1 and 2 due to the train 4SA8 (recorded speed = 32 km/h) including the standard speed-adjusted DLA (bending) in SLS where the stresses are highest at girders' bottom flanges. Figure 11 illustrates recorded maximum stresses (both compressive and tensile) at the installed strain gauges versus the 1st and 2nd principal stresses obtained from the FE Models 1 and 2.

As can be seen, Fig. 11(b) shows that a very good agreement is achieved between the stresses obtained from strain gauges A1, A2, B1 and B2 with the SLS principal stresses in the FE Model 2 when it includes the speed-adjusted DLA (bending) (AS5100.7, Bridge Design Part 7: Bridge Assessment 2017). This means that the FE Model 2 can well represent the actual bridge. The DLAs are taken as recommended

Table 3 Material properties

Material Properties	Steel	Timber Transom (Stress-grade F22 Hardwood) (ETE-09–00, Sect. 9: Structures 2023)
Young's Modulus (MPa)	200,000	16,000
Poisson's Ratio	0.25	0.37
Mass density (kg/m)	7850	650

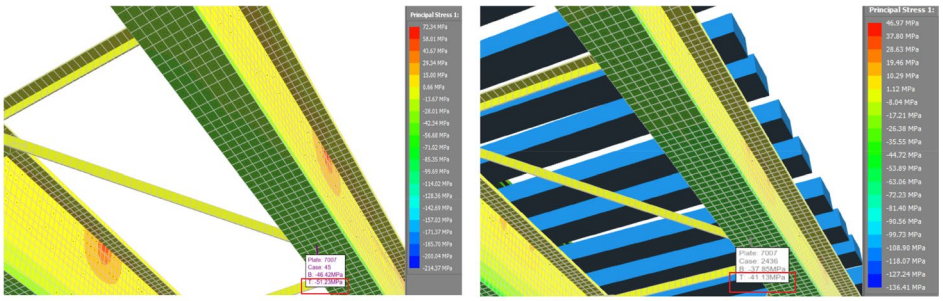

(a) (b)

Fig. 10 Sample contour stress mapping of maximum 1.st principal stress resulted from the analyzed (**a**) FE Models 1 and (**b**) FE Model 2 due to train 4SA8 axle loads (speed = 32 km/h) including design nosing load as recommended by AS5100. Note e.g., plate element 7007 where strain gauge A1/B1 or A2/B2 are installed shows 51.2 MPa and 41.1 MPa in FE Models 1 and 2, respectively. Analyses include the standard speed-adjusted DLA (bending) in SLS. (underside view where all elements are shown as rendered for clarity)

by AS5100.2 (AS5100.2, Bridge Design Part 2: Design loads 2017) rather than vehicle-bridge dynamic response obtained by e.g., a vibration equation or equipment. The DLAs (bending) are adopted from 0.2 to 0.4 depending on the actual speed of trains (Maximum recommended DLA = 0.52). In Fig. 11(b), the maximum error in obtained stresses relates to train 4SA8 with 8.5%. Where FE Model 2 obtains the tensile stress at the bottom of the girder due to train 4SA8 as 41.1 MPa, the actual maximum recorded tensile stress from strain gauge B2 is marginally less i.e., 37.6 MPa. Other stresses are due to other trains being closer to each other. This error is considered to be acceptable as the axle loading reported from the ARTC wayside monitoring may have an error up to ± 3% and DLAs are only taken as standard DLAs which may not fully indicate the real vehicle-structural dynamic response. The ULS in both models is a very high arbitrary level including full standard DLA as well as a load factor of 1.6. Although the stresses at the bottom of girders are in very good agreement with the FE Model 2 principal stress results, the actual stresses obtained in bracings' strain gauges; A3 to A6 and B3 to B6, have significant differences with the principal stresses results in both FE Model 1 and 2. For example, Fig. 11(c) shows that the actual maximum recorded stresses in strain gauges A3 and B3 is 10.2 MPa (compressive). The FE Model 1 in SLS obtains maximum 1st principal stress as 89.1 MPa (compressive) while the FE Model 2 obtains stress as 41.4 MPa (compressive) at the finite plate element where strain gauges are installed. This shows how significantly the actual nosing load is different from the AS5100 single axle in all the models and it proves to what extent AS5100.2 (AS5100.2, Bridge Design Part 2: Design loads 2017) could be conservative for the assessment of existing transom top railway bridges. Even when the transoms are modeled with fully theoretical DoF of fixed constraints in the FE Model 2 with the maximum possible axial and bending stiffness, the compressive SLS stresses (with no load factor and no DLA) in the models are obtained significantly higher than the actual recorded stresses from the strain gauges; meaning that the actual applied lateral loads to this bridge due to different trains are much lower than the modeled concentrated lateral force in reality.

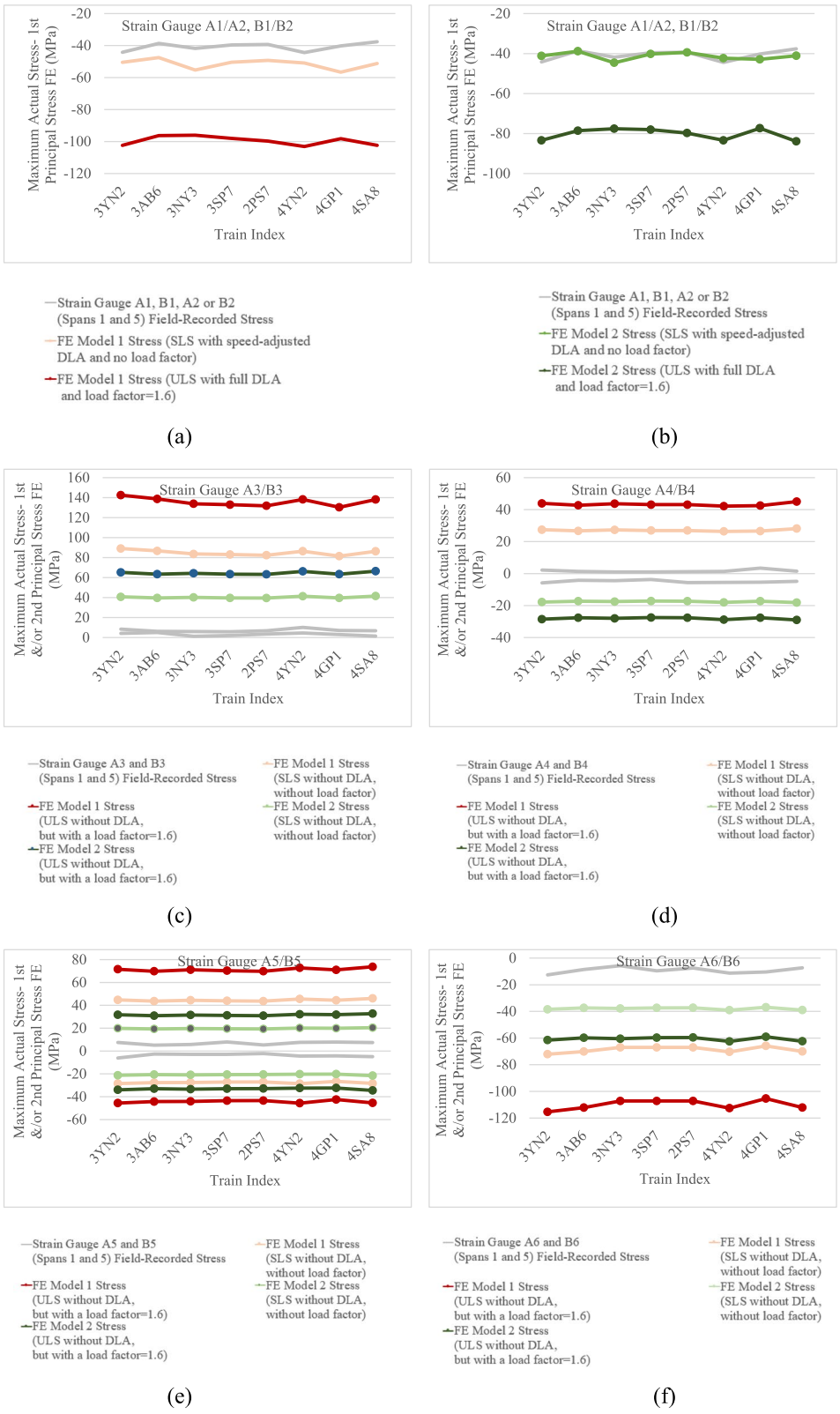

Fig. 11 Maximum recorded stresses in installed strain gauges versus the maximum 1st and/or 2nd principal stresses obtained from the FE Models 1 and 2 (negative and positive numbers show tensile and compressive stresses, respectively)

4 Nosing load estimation

Normally, dynamic or static responses of structures should be obtained to fully update or validate an FE model with field-testing data. In theory, if one could install an unlimited number of accelerometers, they would acquire a full shape of the bridge occurring at each mode of vibration. This data is helpful in validating the natural frequencies and mode shapes of a bridge for various Structural Health Monitoring (SHM) purposes. The vibration data (such as acceleration) can be used together with static responses of the bridge (such as stress, strain, or displacement) to update a FE model through deterministic or stochastic methods (Chen et al. 2022). A common way to validate an FE model without carrying out a complex model updating process is to identify and calibrate modal parameters of a bridge using e.g., modal identification methods and altering structural properties such as Young's modulus, material densities, boundary conditions, members or FE elements constraints/fixities through a rigorous sensitivity-based approach until the FE model represents the actual structure with a good approximation (Ghiasi et al. 2022a, 2022b). It should be noted that as no vibration measurements are available for the current test of this bridge, natural frequencies or mode shapes of this bridge cannot be verified in this research.

In this paper, only stress responses of structures due to passing trains are used to estimate the nosing load. It is worth mentioning that the determination of a lateral load magnitude can further be improved in the future when vibration data is also available and the FE model is updated through rigorous model updating techniques, however, for the purpose of a lateral loading estimation, this level of iteration in stress analysis can sufficiently represent the magnitude of concentrated nosing load due to each train. In this paper, it is assumed that the nosing load is a single lateral point load as prescribed in all the design codes i.e. if the nosing load is not a single point load applied to the top of rails, further research is required to ascertain the type of this load.

The following stages are taken in this paper to reach an acceptable level of FE model validation and nosing load estimation:

4.1 First stage calibration-Stress intensity optimization through controlled lateral loading alterations (Automatic)

This stage is called as 1st calibration hereinafter which is implemented through controlled and automatic lateral load iterations in limited cycles using a developed script in Python and linking that script to Space Gass. This program applies a single nosing load to the rail in FE Model 2, obtains stresses, and optimizes the stress intensities. Mindlin plate theory is used for the force-stress analysis of plates in FE software packages which can be referred to Tessler (1983). The FE stress intensity for the plate P, $\sigma_{i,P}$, due to the nosing force, F_{nos}, can be determined as the largest of the absolute values of the 1st and 2nd principal stresses as below:

$$\sigma_{i,P} = Max(|\sigma_{1,p} - \sigma_{2,p}|) \tag{2}$$

where i defines the stress axis direction, $\sigma_{1,p}$ and $\sigma_{2,p}$ defines the 1st and 2nd principal stress, respectively.

The target here is to optimize $f(\sigma_{i,P})_{k\in(1,n)}$ as below in a controlled number of alterations, k:

$$f(\sigma_{i,P})_{k\in(1,n)} = Min\left|(\sigma_{i,P-FEModel} - \sigma_{i,P-field})\right| \tag{3}$$

where the nosing force, $F_{nos} \in [a, b]$ and $k = 1, \ldots, n$ is the number of loading iterations for nosing load estimation. The initial value range of the nosing load. a and b are the minimum and maximum limit of the loading range which are selected as 17 kN to 26 kN, respectively, based on the actual stress levels obtained in strain gauges A3/B3 to A6/B6 for all the recorded axles.

On the one hand, vertical loads not only induce high stresses in girders' FE plates but also induce some portion of stress in bracings' FE plates due to the flexural torsional buckling of girders' FE plates given the vertical loads are eccentric (rails are not located exactly at the centreline of girders, Fig. 2). On the other hand, lateral loads not only induce high axial compressive stresses in bracings' FE plates but also induce some portion of stress in girders' FE plates (mainly girders' top flange and web) when pushing them inward. In both cases, transom would help in reducing stresses in bracings' FE plates (Fig. 11). Thus, if the eccentric vertical loads do not change and are the same as the vertical moving wheel loads applied to an FE model with the same geometry, the remaining portion of stresses in the bracings' FE plates is due to the change in the lateral nosing force.

It should be noted that the stresses are all in the elastic zone in this paper i.e., there is no requirement for elastoplastic or elastic-elastoplastic mixed loading analysis here; as the stresses obtained in strain gauges A3/B3 to A6/B6 are known to be very low (Fig. 8) and do not reach plates failure levels. Other checks in FE Models demonstrate that the von Mises stresses due to the lateral loading combined with the ordinary-rated vertical axle loads are always obtained much lower than the failure level and linear buckling analysis shows that the buckling is not a case due to such low loads in the analyzed plates.

4.2 Second stage calibration-FE model node constraints alteration and sensitivity analysis (Manual)

The stage is called 2nd calibration hereinafter and is carried out to improve the results obtained from the 1st calibration. As mentioned in Sect. 3, all the transoms in the FE Model 2 are initially modeled as fully fixed constraints (with DoF of FFFFFF) where beams to plates' end nodes are connected with no release in translations and rotations in all directions. However, this may not fully represent the actual constraints of transoms. As mentioned before, it is difficult to adopt true constraints/fixities for each transom in practice without specific field testing because timber transoms may widely vary in boundary conditions, true members' stiffnesses, and physical conditions from one transom to another as well as one bridge to another. However, to obtain a better model calibration from the FE Model 2, the end fixities of the transoms are manually changed until better outcomes are obtained from the model. To do this, the end transoms constraints are set as FFFFFS where $S\ (\theta_{r,tr})$ is the rotational stiffness of transoms in the local z direction of the members (parallel to rails) in each trial. This allows the end-member

transoms' connections to be semi-rigid and transoms can also rotate at connections following their end fixities. The rotational stiffness of the transom, $S(\theta_{r,tr})$, can be expressed as:

$$S = \theta_{r,tr} = \frac{M_{A,tr}}{R_1} \tag{4}$$

where $M_{A,tr}$ is the bending moment applied to joint A at end of a transom and R_1 is rotation (rad) of the semi-rigid connection. A rigorous manual sensitivity analysis is performed to obtain $\theta_{r,tr}$. Results show that the stresses in FE Model 2 get closer to the field-recorded stresses when $\theta_{r,tr}$ is between 900 to 1200 kNm/rad (depending on the location of transoms) rather than when it is considered as fully fixed. It should be noted that no optimization is performed through this manual stage. The validated rotational stiffnesses are adopted for the studied bridge through the FE Model 2. Further checks are also undertaken. Young's modulus of steel is not altered as the stresses in strain gauges are recorded based on the E of steel material as 200,000 MPa. Changes in Young's modulus and material densities of transoms are also carried out in another stage of sensitivity analysis, however, no considerable improvement in the 2nd calibration is achieved by these changes. The actual transoms are F22 type with specified material properties (Table 3) but the stress results in the model are not shown to be very sensitive to the change in Young's modulus or material densities of timber transoms. It is also obvious that changing the model boundary condition would not help in improving the results. Consequently, it is found that the best way to improve the 1st calibration is to change timber constraints as mentioned above.

5 Results and discussion

Figure 12 shows how each calibration improves the results of the FE Model 2. Figure 13 also shows a sample contour mapping of principal stress reduction in FE Model 2 at strain gauge A5/B5 due to the design loading and after the 1st and 2nd calibrations (train 3YN2). Table 4 lists the estimated nosing load for each train for undamaged transoms. In Table 5, the Error is defined as:

$$Error(\%) = \frac{(Stress_{FE} - S_{tressField})}{Stress_{Field}} \times 100 \tag{5}$$

Errors may be reduced through more rigorous model updating methods, however, based on the review of some similar studies in the field of SHM stress analysis and model updating, the errors are deemed to be acceptable for nosing load estimation (Qin et al. 2022a, 2022b). Indeed, the low recorded stresses would result in higher errors between the FE model and field-recorded stresses. Improved error in Table 5 is simply the deduction of 1st and 2nd FE stresses and shows how much errors are improved in the 2nd calibration due to alterations of transom constraints.

As can be seen from Table 5, the percentage of the estimated nosing load to the maximum reported axle load is between 8.6 to 9.4. Depending on the train, the estimated nosing loads are around 3.5 to 4 times less than the assessment nosing load required by AS5100.7 (AS5100.7, Bridge Design Part 7: Bridge Assessment 2017). When comparing these results with the actual comprehensive tests conducted by Otter et al. (Otter

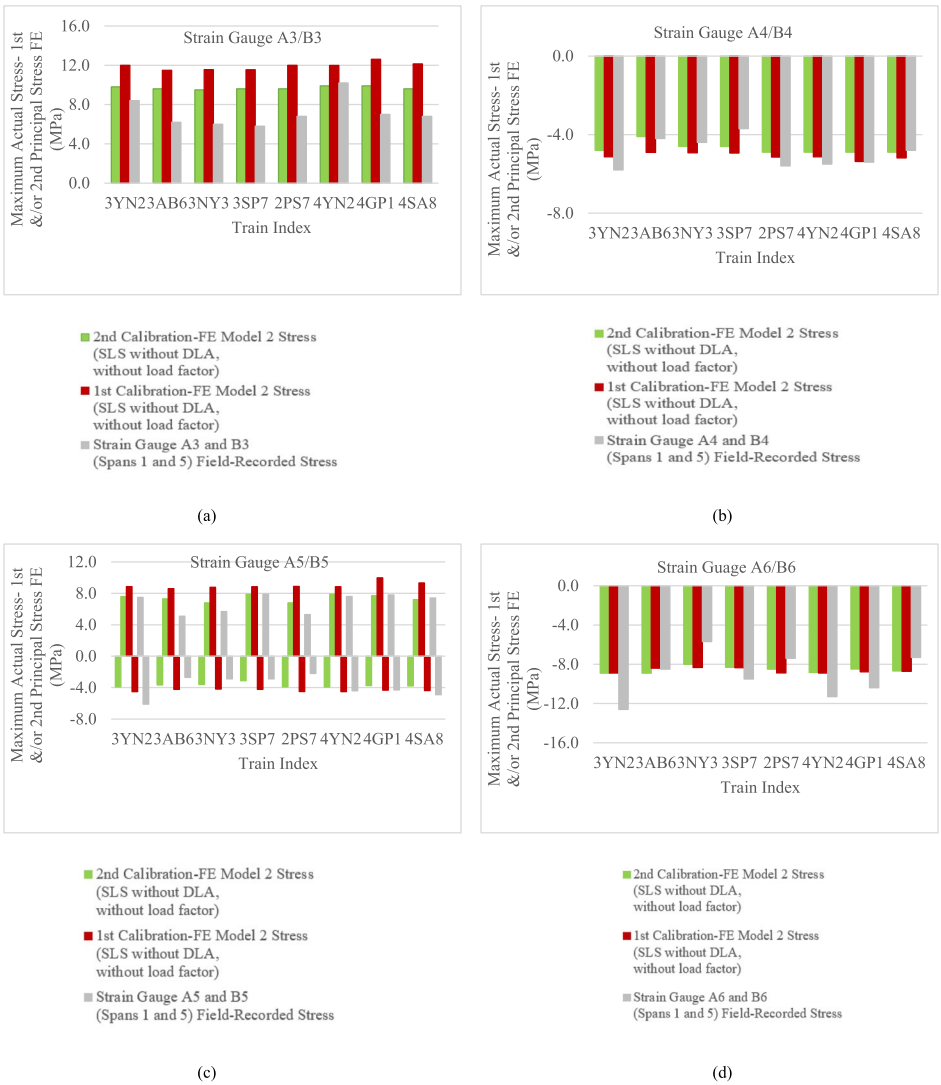

Fig. 12 Maximum recorded stresses at the installed strain gauges versus the calibrated FE Models' maximum 1st and 2nd principal stresses (negative and positive numbers show tensile and compressive stresses, respectively)

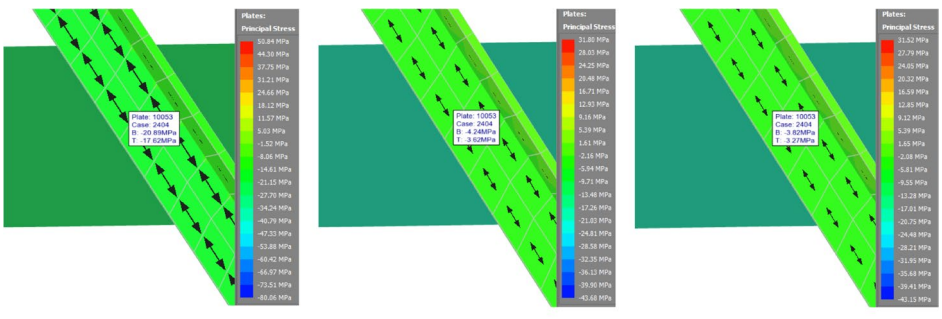

Fig. 13 A sample contour mapping of principal stress reduction at strain gauge A5/B5 where (**a**) shows very high principal stresses due to design loading, AS5100, (**b**) reduced principal stresses after the 1st calibration, and (**c**) further reduced principal stresses after the 2nd. calibration (The wind bracing is shown from the bridge underside)

Table 4 Error (%) between FE Model 2 stress results and field-recorded stresses in both calibrations

Train Index	1st calibration-FE Model 2 Error (%)				2nd calibration-FE Model 2 Error (%)				Improved Error (%) due to the 2nd calibration of FE Model 2			
	A3/B3	A4/B4	A5/B5	A6/B6	A3/B3	A4/B4	A5/B5	A6/B6	A3/B3	A4/B4	A5/B5	A6/B6
3YN2	30.0	-15.9	5.2	-29.4	14.3	-21.3	1.2	-29.4	15.7	5.4	4.0	-0.1
3AB6	46.0	14.5	40.7	-1.3	35.4	-2.4	30.1	-4.7	10.6	16.8	10.6	-6.0
3YN3	48.1	10.8	35.1	31.6	36.8	17.9	16.2	40.4	11.2	-7.2	18.9	-8.8
3SP7	49.7	25.1	10.6	-12.1	39.6	39.4	0.0	-12.5	10.2	-14.3	10.6	0.4
2PS7	43.3	-8.2	40.3	16.7	29.2	14.0	22.1	14.9	14.2	-22.2	18.3	1.8
4YN2	14.9	-6.7	14.1	-21.3	-3.0	0.0	3.8	-21.8	18.0	-6.7	10.3	0.4
4GP1	44.5	-0.6	21.8	-15.7	29.3	-2.0	-1.3	-18.4	15.2	1.4	23.1	2.7
4SA8	44.0	7.5	20.6	16.3	29.2	19.5	-2.8	18.9	14.9	-12.0	23.4	-2.6
Average Improved Error due to the 2nd calibration (%)									**13.7**	**-4.8**	**14.9**	**-1.5**

Table 5 Estimated Nosing point loads for undamaged transoms

Train Index	Estimated Lateral Nosing Load (kN) SLS	Maximum Reported Vertical Axle Load (kN) SLS	Percentage (%) of Lateral to Vertical Load SLS	Estimated Lateral Nosing Load (kN) ULS	Current Required Lateral Nosing Load (kN) ULS AS5100
3YN2	21.0	242.0	8.7	33.6	129.0
3AB6	20.0	231.3	8.6	32.0	123.4
3YN3	20.1	234.3	8.6	32.6	125.0
3SP7	20.2	231.1	8.7	32.3	123.3
2PS7	21.2	230.6	9.2	33.9	123.0
4YN2	21.2	241.5	8.8	33.9	128.8
4GP1	21.5	229.7	9.4	34.4	122.5
4SA8	21.1	242.0	8.7	33.7	129.0

et al. 2005) using load-measuring wheelsets and wayside measurements from TPD and WILD, both tests make very good agreements with each other as Otter et al. obtained that 95% of their recorded lateral forces in all the open-deck bridges were less than 26.7 kN due to vertical axle loads of up to 293.6 kN; meaning that the actual magnitude of their recorded nosing load was only 9.1% of the maximum recorded vertical axle load in their tests.

Transoms in the tested bridge are visually inspected and found to be in reasonable condition (Sect. 2). Accordingly, the modelling assumption is initially based on the theoretical full cross-section transoms. However, this may not be the case for all the bridges anywhere in rail networks (refer to Fig. 1). As the bridge is in service and the actual transoms cannot be damaged for field testing, another investigation is performed in the FE Model 2 (after 2nd calibration) to simulate some cases where the transoms are damaged in different severities. The combined bending and axial stress in a transom in the model, σ_{tr}, can be calculated as the equation below:

$$\sigma_{tr} = \frac{F_{A,tr}}{A_{tr}} + \frac{M_{A,tr} C_{z,tr}}{I_{z,tr}} \tag{6}$$

where $F_{A,tr}$ and $M_{A,tr}$ are the axial force and bending moment applied to joint A at end of a transom respectively, and A_{tr}, $C_{z,tr}$, and $I_{z,tr}$ are a transom's cross-sectional area, the center of gravity and second moment of area around z direction, respectively. Damage severities are incorporated into the model (after the 2nd calibration) as 30%, 60%, and 90% to increase σ_{tr} by reducing A_{tr} and $I_{z,tr}$ in the FE model to reflect the effect of damaged timber transoms. For this purpose, the stresses at A3/B3 to A6/B6 strain gauges are obtained in the FE model when damaged transoms are incorporated in the FE model and then these new stresses are compared with the stresses in the undamaged FE model when 56% of an AREMA's nosing load is applied to the FE model. As mentioned in Sect. 1, the recommended AREMA (Engineering et al. 1997) nosing load is one-quarter of the maximum vertical axle load in ASD. Fifty-sixth percent of this load is applied to adopt a case e.g., if this load is taken in ULS when the axial capacity reduction factor is also taken as 0.9 as per AS5100.6 (AS5100.6, Bridge Design Part 6: Steel and Composite Construction 2017) ($1 \times 0.9/1.6 = 0.56$ or 56%). Such AREMA's loads vary between 32.2 kN for train 4GP1 to 33.9 kN for train 3YN2 which are 50% and 61% higher than the

estimated nosing loads in Table 5. Figure 14 shows the results of all the FE models when new stresses due to the damaged transoms in A3/B3 to A6/B6 are obtained from the FE model and these stresses are compared with stresses due to AREMA's nosing load.

As can be seen from Fig. 14, all the stresses when the FE model incorporates damaged transoms are well lower than the principal stresses due to AREMA's SLS-adopted nosing load. It is illustrated that the obtained stresses from the FE model are more sensitive to the nosing load than the damage severities in timber transoms, however, this practice is to ensure the nosing load is also estimated where damages are incorporated in the FE model. It is concluded that for nosing load assessment of the transom top bridges, AREMA (Engineering et al. 1997) recommended nosing load can be used with a load factor of unity i.e., a maximum ULS factored single load of 75 kN in ULS for 300LA or equivalent axle-adopted lateral load for lower vertical

Fig. 14 Maximum FE principal stresses at the installed strain gauges (damage incorporated in the FE model with various severities) versus FE principal stresses due to AREMA's SLS-adopted nosing load

loads (e.g., 62.5 kN nosing load in ULS for the maximum vertical axle load of 250 kN) as the worst case nosing load scenario without any further investigation to ensure no unnecessary expensive costs is imposed to rail authorities. As illustrated in Fig. 14, even the recommended SLS-adopted nosing load would obtain 18% to 81% higher stress results than the ULS stresses due to the actual recorded nosing load. Because the assessment of existing transom top bridges is always based on visual and detailed inspection (AS5100.7, Bridge Design Part 7: Bridge Assessment 2017), the above assessment load can ensure that no extensive and expensive wind bracing upgrades or strengthening is imposed on rail authorities where there is no sign of distress in wind bracings. Although the above results are obtained for transom top bridges, the results from this paper can also be applied to any other railway bridges such as U-Frame ballast top or open deck, or any other railway bridges when wind bracings are required to be assessed against nosing load.

6 Conclusion

This paper has estimated the actual nosing loads applied from various trains to an existing railway transom top bridge using field-recorded stresses and validated FE models of the bridge through a two-staged model validation approach including both the automatic stress intensity optimization and rigorous manual FE model sensitivity analysis. Damaged transoms with various severities have also been incorporated into the FE model when their constraints have been validated through the model validation process. Results have demonstrated that the actual stresses in wind bracings of the tested railway transom top bridge are significantly lower than the stresses that are induced by the required assessment load of the AS5100. The actual nosing loads have been estimated with magnitudes ranging only between 8.6% to 9.4% of the maximum vertical axle load of the passed trains. Both field-recorded and validated FE model stresses have suggested that the required AS5100 nosing load for bridge assessment should be revised to avoid expensive and unnecessary upgrades of numerically assessed deficient wind bracings. It has been demonstrated that the AREMA's recommended nosing load i.e., a lateral point load as one-quarter of the maximum vertical axle load can be used with a load factor of unity in ULS assessment level without further investigation after visual structural confirmation of wind bracing condition in existing railway transom top bridges.

Acknowledgements
The authors would like to acknowledge the Australian Rail Track Corporation (ARTC) for their authorization in accessing and field testing of the Menindee Darling River Railway Bridge site as well as the permission to include available bridge information and drawings in this paper. The authors would also like to thank Mr. Henry Griscti and Mr. Cameron Abraham for assisting and undertaking the field data collection, equipment setup, and testing management during the field testing week. The authors also thank Mr. Anthoney Bird for their support and technical overview of the undertaking works.

Authors' contributions
Alireza Ghiasi (AG): Writing–Original Draft, Conceptualization, Methodology, All Testings, Analysis and Validation. Daniel Lee (DL): Supervision, Field Testing, Review, and Editing.

Funding
This research received no external funding.

Availability of data and materials
All the datasets used and analyzed during the current study are available from the corresponding author upon reasonable request.

Declarations

Competing interests
The authors declare that they have no known competing financial interests or personal relationships that could have appeared to influence the work reported in this paper.

Received: 6 February 2024 Accepted: 5 April 2024
Published online: 01 June 2024

References

American Railway Engineering and Maintenance-of-Way Association (AREMA) Part 2: Railroad Bridge Design, 1997.
AS5100.2, Bridge Design Part 2: Design loads, Australian Standard, 2017.
AS5100.6, Bridge Design Part 6: Steel and Composite Construction, Australian Standard, 2017.
AS5100.7, Bridge Design Part 7: Bridge Assessment, Australian Standard, 2017.
AS7636, Railway Structures, RISSB Rail Industry Safety and Standards Board, 2022.
AS 1085.1, Railway Track Materials Part 1: Steel rails, Australian Standards, 2002.
A. Prud'homme, Resistance of the Track to Lateral Loads Exerted by Rolling Stock, Revue Generale des Chemins de Fer, 1967.
Chen SZ, Zhong QM, Hou ST, Wu G (2022) Two-stage stochastic model updating method for highway bridges based on long-gauge strain sensing. Structures 37:1165–1182
S. Deng, A simplified model for assessing lateral railway bridge resonance behaivior, 2015.
EN 1991–2, Eurocode 1: Actions on Structures, 2006.
ETE-09–00, Section 9: Structures, Australian Rail Track Corporation-ARTC, 2023.
ETE-09–05, Section 9: Load Rating of Underbridges, Australian Rail Track Corporation-ARTC, 2022.
L. Georgiev, V. Tanev, L. Zdravkov, Equivalent nosing force for a steel railway bridge based on in situ measurements, IABSE Congress Ghent, 2021.
Ghiasi A, Moghaddam MK, Ng CT, Sheikh AH, Shi JQ (2022a) Damage classification of in-service steel railway bridges using a novel vibration-based convolutional neural network. Engine Struct 264:114474
Ghiasi A, Ng CT, Sheikh AH (2022b) Damage detection of in-service steel railway bridges using a fine k-nearest neighbor machine learning classifier". Structures 45:190–1935
Hughes TJ, Tessler A (1983) An improved treatment of transverse shear in the Mindlin-type four-node quadrilateral element. Comp Methods Appl Mech Engine 39:311–335
D. Jastrzebski (1959) Nature and Properties of Engineering Materials. Wiley, Michigan
L.T. James, G.A. Scott (1994) Parametric study, Lateral Forces on Railway Bridges. UIC, Paris
Khatibi F, Esaeili M, Mohammadzadeh S (2017) DEM analysis of railway track lateral resistance. Soils Found 57:587–602
Lateral Resistance of Railroad Track, U.S. Department of Transportation, 1977, FRA/ORD-77/41.
McLean DI (1998) ML Marsh. Dynamic impact factors for bridges, Washington
A. Miri (2022) Mitigating severity of longitudinal interaction of rail-track-bridge system in transition zones for safer trains. Queensland University of Technology, Queensland
Mirza O, Shill SK, Johnston J (2019) Performance of precast prestressed steel-concrete composite panels under static loadings to replace the timber transoms for railway bridge. Structures 19:30–40
F. Moreu, A. M. Rokoczy, M. Sanaie Lateral Loads and Displacements of Railroad Bridges from Field Investigations, ASCE-Bridge Engineering, 2023, https://doi.org/10.1061/5982.
F. Moreu, J. M. LaFave, Railroad Bridges and Structural Engineering, Department of Civil and Environmental Engineering University of Illinois at Urbana-Champaign, 2012, 1940–9826. https://core.ac.uk/download/pdf/10201376.pdf.
D. Otter, B. Doe, S. Belport, Rail Car Lateral Forces for Bridge Design and Rating, Technology Digest, 2005, TD-05–002.
Part 1030, Rail Structures, Department for Infrastructure and Transport, 2007.
Pipinato A, Patton R (2015) Innovative Bridge Design Handbook- Construction. Elsevier, Rehabilitation and Maintenance
Qin S, Han S, Li S (2022a) In-situ testing and finite element model updating of a long-span cable-stayed bridge with ballastless track". Structures 45:1412–1423
Qin S, Yuan Y, Han S, Li S. A Novel Multiobjective Function for Finite-Element Model Updating of a Long-Span Cable-Stayed Bridge Using In SituStatic and Dynamic Measurements." ASCE-Bridge Engineering 2022 https://doi.org/10.1061/1943-5592.0001974.
T HR CI 12008 ST, Capacity Assessment of Underbridges, Transport for NSW, 2019.
TMC 311, Transoms, RailCorp Engineering Manual, 2010.
WisDOT Bridge Manual, Chapter 38: Railroad Structures, 2019.
Zakeri JA (2012) Lateral Resistance of Railway Track. Iran University of Science and Technology, IntechOpen

Publisher's Note